PHYSICAL REVIEW B **84**, 184203 (2011)

Low-temperature structure of ξ'-Al-Pd-Mn optimized by *ab initio* methods

Benjamin Frigan,[1,*] Alejandro Santana,[2] Michael Engel,[3] Daniel Schopf,[1] Hans-Rainer Trebin,[1] and Marek Mihalkovič[4]

[1]*Institut für Theoretische und Angewandte Physik, Universität Stuttgart, DE-70550 Stuttgart, Germany*

[2]*Grupo de sistemas complejos, Universidad Antonio Nariño, Bogotá, Colombia*

[3]*Department of Chemical Engineering, University of Michigan, Ann Arbor, Michigan 48109, USA*

[4]*Institute of Physics, Slovak Academy of Sciences, SK-84511 Bratislava, Slovakia*

(Received 8 September 2011; revised manuscript received 19 October 2011; published 14 November 2011)

We have studied and resolved occupancy correlations in the existing average structure model of the complex metallic alloy ξ'-Al-Pd-Mn [Boudard *et al.*, Philos. Mag. A **74**, 939 (1996)], which has approximately 320 atoms in the unit cell and many fractionally occupied sites. Model variants were constructed systematically in a tiling-decoration approach and subjected to simulated annealing by use of both density functional theory and molecular dynamics with empirical potentials. To obtain a measure for thermodynamic stability, we reproduce the Al-Pd-Mn phase diagram at $T = 0$ K, and derive an enthalpy of formation for each structure. Our optimal structure resolves a cloud of fractionally occupied sites in pseudo-Mackay clusters. In particular, we demonstrate the presence of rotational degrees of freedom of an Al_9 inner shell, which is caged within two icosahedrally symmetric outer shells Al_{30} and Pd_{12}. Outside these clusters, the chemical ordering on a chain of three nearby sites surprisingly breaks the inversion symmetry of the surrounding structure, and couples to an Al/vacancy site nearby. Our refined tiling-decoration model applies to any structure within the ε-phases family, including the metastable decagonal quasicrystalline phase.

DOI: 10.1103/PhysRevB.84.184203 PACS number(s): 61.44.Br, 61.50.Ah, 61.50.Lt, 71.15.Nc

I. INTRODUCTION

The ternary Al-Pd-Mn system is of great interest for the study of physical properties of quasicrystals and their approximants. Its phase diagram contains both a stable icosahedral phase and a stable decagonal phase in the vicinity of various other crystalline approximants, many of which can be grown as single crystals with high perfection. Of particular interest is the series ξ', ξ'_1, ξ'_2, ... of orthorhombic approximants[1] of the icosahedral quasicrystalline alloy i-Al-Pd-Mn, which exists in the Al-rich corner of the phase diagram.[2] An alternative notation for these phases is ε_l, $l = 6,16,28,\ldots$, where l denotes the strong $(0,0,l)$ diffraction spot for the interplanar spacing. ξ'_2 (ε_{28}) is frequently named Ψ phase. All these phases have a common periodicity of 16 Å along (0,1,0) and can be described as two-dimensional tilings perpendicular to that direction.[1] For the ξ' phase (ε_6) the tiling consists of staggered flattened hexagon tiles, where occasionally *phason defects* can show up composed of a nonagon and pentagon tile.[3] There is a similar structure where the hexagons are all parallel, denoted ξ. In the ξ'_n phases, the phason defects are arranged in rows, called *phason planes* and squeezed in between $n-1$ rows of hexagons forming a layered superstructure.

The most recent experimental structure refinement of ξ' was conducted in 1996 by Boudard *et al.*[4] The close relationship between ξ and ξ' was studied by Klein *et al.* via high resolution electron microscopy.[3] So far no structure refinement of the ξ'_n phases has been reported in the literature, but the tiling representation allows us to extend structure models for ξ and ξ' to structure models of ξ'_n. Important building blocks of all structures are pseudo-Mackay icosahedral clusters (PMI) which form columns parallel to (0,1,0) and when projected are the vertices of the tiling representation discussed above. The PMI shares the outer shells (Pd_{12} icosahedron and Al_{30} icosidodecahedron) with the conventional Mackay icosahedron (MI) cluster, while the inner shell, an Al_{12} icosahedron in the MI, is replaced by a less symmetric shell of 8–10 Al atoms. While the positions of the outer shells are predicted with high accuracy from diffraction data, the positions of the inner Al atoms are less well defined and have large uncertainties: in experiment, the inner sites are characterized by mixed and partial occupancies;[4] when projected from a hyperspace model they correspond to positions close to the boundary of atomic surfaces,[5] which suggests that they might be intrinsically unstable.

Interest in the ξ'_n phases has spurred when Klein *et al.*[6] discovered a special texture around a partial dislocation of Burgers vector 1.83 Å.[7] On the tiling level,[8] the dislocation results in the insertion of six phason planes of width ≈171 Å, which means it can alternatively be viewed as a dislocation in the layered superstructure. The dual nature of the dislocation—on the atomic level and on the tiling level—and the resulting hierarchy in length scales lead to the adoption of the term *metadislocation* for this special class of dislocations.[6] Metadislocations are known to be important for the plasticity of the ξ'_n phases,[6,9,10] but so far little is known about the atomistic structure of the metadislocation core and the details of the metadislocation motion. A refined atomistic structure model of the underlying crystal phases as achieved in this work can form the basis of a better understanding of these two aspects.

In this contribution we report a structural refinement of the Boudard model of ξ' via numerical optimization. Simulated annealing with molecular dynamics and empirical potentials, and density functional theory, are used to relax the structure into its energy minimum. We derive an enthalpy of formation for each model and compare it with the enthalpy of other phases coexisting in the Al-Pd-Mn system. This yields a direct measure for thermodynamic stability. We identify two main sources of disorder that plagued a direct structural determination of the structure from the diffraction data. One type of

disorder is related to the symmetry-broken inner shell of the PMI cluster. The symmetry breaking of this shell, along with extra space due to the vacated sites, leads to a low-temperature state described by an ensemble of configurations, instead of the unique icosahedral one. Individual representatives of this ensemble are *a priori* not accessible to experimental diffraction refinements, which only captures the average structure. We discuss how such an average structure may even become ill-defined due to missing strong intracluster and intercluster occupancy correlations. The second source of disorder mixes vacancies, Pd and Al atoms in the interstitial parts of the structure, not covered by any PMI cluster.

The symmetry-broken PMI inner-shell configurations may acquire special importance due to their potential impact on the long-range ordering in quasicrystals. For it is exactly these atoms that define boundaries of polyhedral atomic surfaces defining perfect quasicrystal structures in six-dimensional hyperspace.[11] While there is probably no hope to accurately determine such individual configurations *in situ* in the quasicrystal phase, crystal structures like the ξ' phase studied here present a unique opportunity to study these configurations without the need of modeling a quasiperiodic quasicrystalline structure.

The paper is organized as follows. After a description of the initial model and simulation methods in Secs. II and III, respectively, we present details of our results in Sec. IV: first, a low-temperature Al-Pd-Mn phase diagram is presented in Sec. IV A, which forms the basis for our stability evaluations. The optimization of the ξ' phase and the rotational degrees of freedom of the inner PMI shells are discussed in Secs. IV B and IV C. Finally, in Sec. V a comparison is made with the isostructural Al_3Pd phase, and first structure models for the phason defects are presented. We conclude with a short summary in Sec. VI.

II. AVERAGE STRUCTURE OF ξ': THE BOUDARD MODEL

The space group of the ξ' phase was determined by Boudard *et al.*[4] as *Pnma* (No. 62).[12] The unit cell contains about 320 atoms with a composition around $Al_{73.5}Pd_{22.4}Mn_{4.1}$. The lattice parameters are $a = 23.54$ Å, $b = 16.57$ Å, and $c = 12.34$ Å. The structure exhibits a large amount of disorder. Only 19 of 48 atomic sites are fully occupied, whereas 15 sites possess occupancy factors of 0.5 or less.

The average structure of ξ' consists of two types of atomic clusters, the PMI and the so-called large bicapped pentagonal prism (LBPP). The clusters are illustrated in Fig. 1. The PMI cluster is formed by a symmetry-broken (relative to the approximate icosahedral symmetry of the outer shell) inner shell, which accommodates 8–10 Al atoms. Most of the atoms form short (2.35–2.5 Å), presumably strong bonds with the central Mn atom. This inner shell is encaged by the nearly icosahedral second shell, forming apparently favorable Al-Pd patterns with Pd atoms. The second shell is composed of a large Pd_{12} icosahedron with a radius of 4.44 Å, and of an Al_{30} icosidodecahedron with an approximate radius of 4.9 Å. Both Al and Pd subshells of the second shell have only about 0.14 Å radial deformation. The significance of this cluster is clearly evidenced by the 1.5 Å gap separating the second shell from the outer atomic structure.

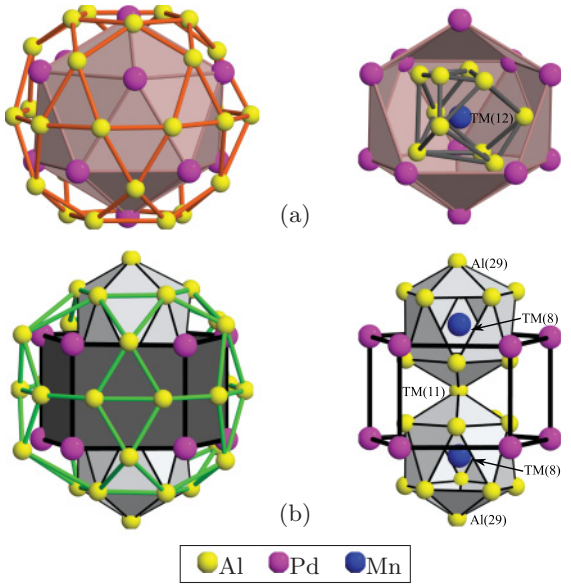

FIG. 1. (Color online) Atomic clusters in ξ'. (a) PMI cluster consisting of a centered Mn atom, a symmetry-broken inner Al shell, a Pd icosahedron, and an Al icosidodecahedron. (b) LBPP cluster composed of two Mn-centered Al icosahedra which are capped within a Pd pentagonal prism, and an Al icosidodecahedron-type shell. Atomic coordinates and labeling is taken from Ref. 4. Note that in these pictures all atomic sites are fully occupied.

The PMI clusters cover almost 90% of the structure. All remaining atoms can be ascribed to a LBPP cluster. Despite its nearly perfect pentagonal symmetry, this cluster also consists of two nearly spherical shells, that are well separated from each other, and also from the outer structure. Here, the first-neighbor distances to the central atom range from 2.6 to 2.8 Å for the inner $Al_{10}Mn_2$ shell. The outer $Pd_{10}Al_{32}$ shell has about the same radii as the second shell of the PMI cluster (4.6 Å for Pd atoms, 5.0 Å for Al atoms), with a bigger radial distortion (about 0.3 Å) for the Al subshell. It is still well separated from the outer shell, which starts at approximately 6.5 Å. Only nine atoms of the LBPP cluster are not shared with any adjacent PMI.

The PMI clusters are stacked on top of each other forming cluster columns along the **b** direction. Connecting adjacent columns results in a two-dimensional tiling consisting of flattened hexagons with an edge length of about 7.6 Å. Figure 2(a) shows a cut through the structure perpendicular to the stacking axis. The LBPP clusters are located inside the hexagons and are arranged in a zig-zag pattern along the **b** direction as shown in Fig. 2(b).

This description comprises more than 98% of the atoms in the structure. Only two Al atoms per hexagon (per unit cell height) cannot be attributed to any cluster.

The structure can be divided into three fundamental layers perpendicular to the stacking axis: a flat (F) layer which is a mirror plane, a puckered (P) layer, and an inverse (I) layer which contains the inversion center. The remaining layers in Fig. 2(b) are obtained through symmetry operations of the

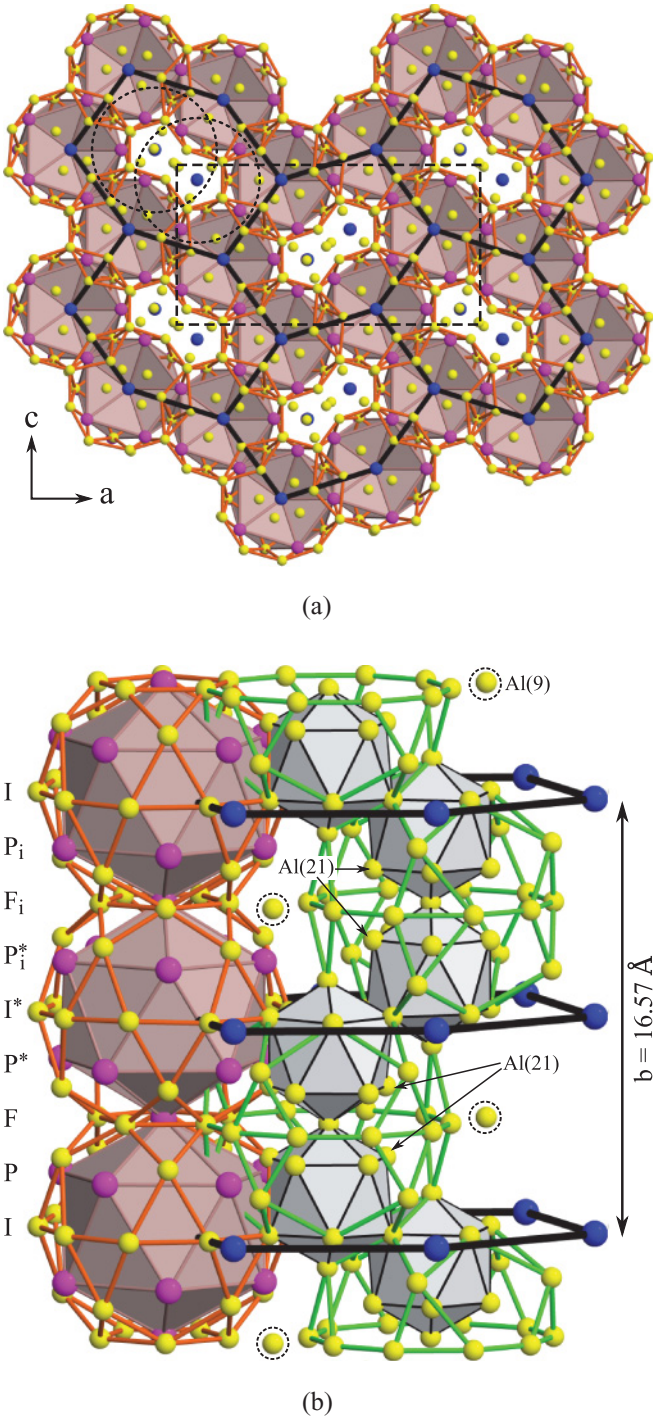

FIG. 2. (Color online) Alignment of the atomic clusters in ξ'. (a) Projection of the structure along the stacking axis of the PMI clusters. Black lines connect adjacent PMI-cluster columns. Dashed rectangle outlines the unit cell, dotted circles indicate the positions of the LBPP clusters. (b) Side view of one flattened hexagon. For the sake of simplicity, only one PMI column is shown. The Pd_{10} pentagonal prisms are omitted from the LBPP clusters in this picture. The "free" Al atoms not covered by any cluster are encircled by black-dashed lines.

space group. The subscript i denotes inverse images with respect to the I layer, and the asterisk symbolizes mirror images with respect to the F layer.

III. METHODS

A. Tiling-decoration model

Our goal was to replace the average structure determined from x-ray diffraction with many fractionally occupied or mixed sites by an ensemble of configurations, each of which is a valid configuration with plausibly low energy. Alternatively, recognizing the hierarchical organization of the average structure in clusters that fill the space following precisely obeyed linking rules, our initial starting models are constructed by a tiling-decoration method. The method creates a unique one-to-one correspondence between tilings and atomic structures.[13] This is achieved by the decoration step: each tile, or more precisely each predefined tiling object (node, linkage, tile interior, etc.) carries an identical atomic motif associated with the considered structure. Consequently, we can refine positional parameters that are associated with each decorated tiling objects in a manner analogical to the refinement of Wyckoff positions in a unit cell of a crystal. The long-range order of a tiling-decorated structure is then defined by the underlying tiling.

One benefit of this approach is a straightforward use of the ξ phase as a replacement of the twice as big ξ' phase in the refinement process: we simply refine the decoration motifs in ξ by total energy calculations, and afterwards substitute the underlying tiling representing ξ by a tiling representing ξ'. The tilings for ξ and ξ' are shown in Fig. 3. In both cases the fundamental tiles are boat tiles (discussed below), packed either in parallel (ξ) or antiparallel (ξ') order.

Decoration rule for the tiling. We associate columns of PMI clusters with the "large" *nodes* of the binary Penrose tiling (BPT).[14] The zig-zag columns of the LBPP clusters project exactly as "small" vertices of the BPT. We find that the atomic motifs are in fact consistent with a particular subset of rhombic BPT family, namely the so-called hexagon-boat-star (HBS) tiling. As shown in Fig. 3, the ξ and ξ' phases are pure boat tilings with no hexagon or star tiles. The Penrose rhombi, into

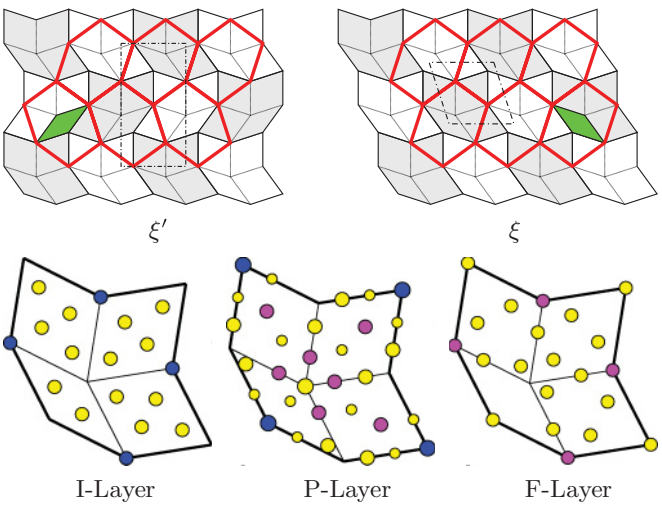

FIG. 3. (Color online) Top: HBS tiling models for ξ and ξ'. Red (thick) lines connect adjacent PMI-cluster columns. Unit cells are highlighted with dash-dotted lines. Bottom: Tiling-decoration rule for the boat tiles reproducing the Boudard model. Larger circles indicate atoms sitting in lower layers.

which the H, B, and S tiles can be uniquely decomposed, have an edge length of about 6.6 Å. We chose a stacking period of 16.5 Å for all structures. The initial decoration rule for the boat tiles in the ξ and ξ' tiling was set to closely reproduce the atomic structure found by Boudard *et al*. We decorate the tiles for each atomic layer separately. It only is necessary to set up decoration rules for the three fundamental layers I, P, and F, and align them along the stacking axis (I at 0.0, P at 0.125, and F at 0.25, in units of the unit cell height). The decoration rules for the other layers are obtained through symmetry operations applied to columnar atomic motifs bound to our set of tiling objects. Our decoration rules relating the Boudard model of ξ' to the boat tiles are shown in Fig. 3.

A generalization of these pure-boat tiling models to the family of HBS tilings requires us to optimize one more decoration motif, occurring in the hexagon tile, when a pair of skinny rhombi shares a common edge. In our case such a situation leads to a new type of horizontal interaction between the LBPP clusters, and must therefore be optimized separately. This final decoration rule was optimized (see Sec. V B), and we believe it describes faithfully the atomic structures corresponding to the various experimentally observed tiling patterns.[1]

B. Total energy calculations

The total energy of a structure is obtained using a combination of classical molecular dynamics and density functional theory (DFT). First, the candidate structure is relaxed into its global energy minimum in a molecular dynamics annealing approach. Typically, the sample is heated up to 1000 K and slowly cooled down to 0 K. We found that an annealing time of about 50 ps is sufficient for our purposes. The annealing simulations are performed with the ITAP molecular dynamics program IMD in the NVT ensemble.[15] Atomic interactions are modeled with the embedded atom method (EAM).[16] Suitable potentials have been developed for this work with the force-matching method[17] using the POTFIT program.[18] A detailed account of the procedure can be found in Ref. 19.

The final total energies are calculated with the Vienna *ab initio* simulation package VASP.[20,21] Our calculations employ the projector-augmented wave (PAW) method[22,23] in the Perdew-Wang generalized gradient approximation (PW91-GGA).[24] The Brillouin zone is sampled with a Monkhorst-Pack grid.[25] The *k*-point density is chosen in such a way that all energies converge to a precision of 10^{-3} eV. Using a conjugate gradient algorithm, atomic positions as well as the shape and size of the unit cell are relaxed once more, until an accuracy of 10^{-3} eV or better is reached.[26] All calculations are performed with a constant plane-wave energy cutoff of 269 eV.

To assess a low-temperature Al-Pd-Mn phase diagram, we calculate total energies of all experimentally known stable phases including its binary and pure elemental subsystems. We define the enthalpy of formation ΔH as the difference of the total energy of a structure relative to the composition-weighted total energies of its pure elements. Using the program QHULL,[27] a convex hull of enthalpy versus composition is calculated. Structures that minimize the enthalpy are considered thermodynamically stable (at $T = 0$ K). These phases constitute the vertices of the convex hull. Edges and facets indicate two-phase and three-phase regions, respectively. Structures with ΔH above this "enthalpy surface" are unstable. The energy difference ΔE to the convex hull indicates their degree of instability. More details of similar VASP and convex hull calculations can be found, for instance, in Refs. 28 and 29.

When comparing unrelated structures, our target accuracy for the total energies is 1 meV/atom, and this accuracy is certainly guaranteed by our convergence criteria. In our experience, using for example the Perdew-Burke-Ernzerhof generalized gradient approximation (PBE-GGA),[30] the energy differences ΔE from PW91-GGA are usually reproducible to within 1–3 meV/atom. However, when it comes to comparing energy differences for variants of the same structure, the energy differences should not, in general, be divided by the number of atoms, since they only reflect differences in particular places of the structure. Such energy differences can be reliably evaluated with much higher accuracy than 1–3 meV/atom.

IV. RESULTS

A. Low-temperature Al-Pd-Mn phase diagram

The binary Al-rich Al-Mn and Al-Pd phases are the main constraints for the formation of Al-rich ternary phases. In the following, we first discuss the binary subsystems as well as all previously known stable ternary phases. These phases are summarized in Table I along with the elementary subsystems. Figure 4 shows the zero-temperature "energy-phase diagram" in the Al-rich corner without our optimized ξ' phases.

Al-Pd binary phases. The stable Al-rich phases are Al_4Pd, $Al_{21}Pd_8$, Al_3Pd_2, and AlPd.[31] The latter is a FeSi-type

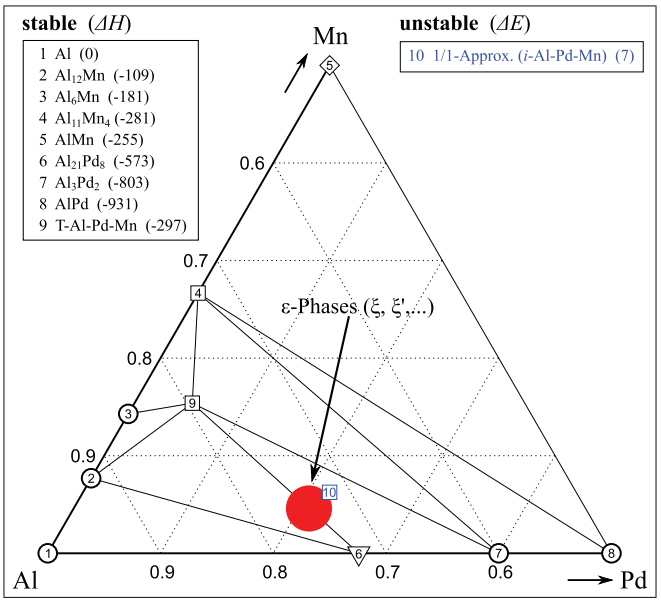

FIG. 4. (Color online) The Al-Pd-Mn energy-phase diagram in the Al-rich corner at $T = 0$ K. Circles label known stable binary phases, diamonds indicate known metastable phases, squares are either unreported or unknown structures, and triangles correspond to high-pressure phases. Tie lines connect low-enthalpy phases, constituting the convex hull vertices. Enthalpies ΔH and energy differences ΔE to the convex hull are given in parentheses in meV/atom. The red spot outlines the approximate compositions of the ε phases.

TABLE I. Low-temperature phases in the Al-rich corner of the Al-Pd-Mn phase diagram (cf. Fig. 4).

	Structure	Space group (No.)	Pearson symbol	Total energy (eV/atom)
1	Al	$Fm\bar{3}m$ (225)	$cF4$	−3.688
–	Pd	$Fm\bar{3}m$ (225)	$cF4$	−5.199
–	Mn	$I\bar{4}3m$ (217)	$cI58$	−8.963
2	$Al_{12}Mn$	$Im\bar{3}$ (204)	$cI26$	−4.202
3	Al_6Mn	$Cmcm$ (63)	$oC28$	−4.623
4	$Al_{11}Mn_4$	$P\bar{1}$ (2)	$aP15$	−5.372
5	AlMn	$P4/mmm$ (123)	$tP4$	−6.581
6	$Al_{21}Pd_8$	$I4_1/a$ (88)	$tI116$	−4.674
7	Al_3Pd_2	$P\bar{3}m1$ (164)	$hP5$	−5.091
8	AlPd	$P2_13$ (198)	$cP8$	−5.369
9	T-$Al_{31}Pd_2Mn_6$	$Pnma$ (62)	$oP156$	−4.873
10	1/1−i-$Al_{23}Pd_7Mn_2$	$P2_12_12_1$ (19)	$oP128$	−4.863

structure. The usual $B2$-type phase (CsCl) with the same composition becomes stable only at high temperature. Al_3Pd_2 is an ordered-vacancy state related to $B2$-AlPd, where each Pd atom has only three Pd nearest neighbors. The $Al_{21}Pd_8$ phase has a more complex structure, and an Al-content similar to the ξ' phase. One efficient structural diagnostics for Al-rich Al-TM (transition metal) compounds is to look at the local environments of the TM atom. These structures often seek to maximize the number of Al-TM bonds. TM atoms tend to have a few or no TM nearest neighbors. Looking at the environments of all TM atoms, (almost) all atoms of the structure are represented. Both Pd sites in $Al_{21}Pd_8$ have a very similar local environment of ten Al atoms. These local environments are reminiscent of the inner Al shells in the PMI clusters of the ξ' phase.

While the λ-Al_4Pd phase is reported as a stable Al-Pd compound,[32] its structure has never been determined. However, the recently determined structure of the Al_4Pt was conjectured to be isostructural with it.[33] Substituting Pt for Pd in this hexagonal structure, and resolving obvious correlations between four fractionally occupied Al sites, we find two variants of this phase just slightly unstable (by about 5 meV/atom) against decomposition to fcc Al and $Al_{21}Pd_8$. The structure of Al_4Pd is similar to the $Al_{21}Pd_8$: both are packings of similar $Al_{10}Pd$ clusters.

At high temperature, the ξ' phase extends into the Al-Pd binary system.[34–36] In Sec. V A an optimized low-temperature structure model for Al_3Pd is presented and compared with the ξ' phase.

Al-Mn binary phases. The evaluation of phase stabilities in the Al-Mn binary phase diagram (based on *ab initio* total energy calculations) results in two suboptimally resolved phases: (i) Al_8Mn_5 phase: it is difficult to refine simultaneously the Al-Mn chemical ordering along with a magnetic structure; (ii) μ-Al_4Mn contains approximately 570 atoms in a hexagonal unit cell. Due to the reported mixed/partial occupancies, an optimization of the low-temperature structure presents a significant challenge to the available computational resources. Thus, our calculated Al-Mn convex hull includes four phases: $Al_{12}Mn$ ($Al_{12}W$ prototype), Al_6Mn, $Al_{11}Mn_4$, and tetragonal AlMn.[37] Out of these, the lowest formation enthalpy ΔH is achieved by the $Al_{11}Mn_4$ phase, while Al_6Mn and $Al_{12}Mn$ enthalpies are barely below the tie line connecting $Al_{11}Mn_4$ with fcc Al.

Since the ξ' phase (and all other ε phases) is located closer to the Al-Pd binary system in the phase diagram, we believe that the Al-Mn binary system has a smaller impact on these phases. Even though the Al_4Mn and Al_8Mn_5 phases are refined only suboptimally, the lowest-enthalpy structure is $Al_{11}Mn_4$. It has also a more similar Al content to ξ', and should therefore be the most important Al-Mn phase to consider.

Previously known stable ternary phases include the icosahedral[38,39] and the decagonal[40] quasicrystalline phases, the ξ' phase, and the so-called T phase, an approximant of the decagonal phase with 12 Å stacking period.[41,42] The ξ' phase has a composition similar to the icosahedral phase, and has been treated as its approximant.[5] At the same time it is a proper approximant of the decagonal phase with 16 Å periodicity.

The stable icosahedral quasicrystalline phase has a composition of $Al_{71.1}Pd_{20.2}Mn_{8.7}$.[43] Here we represent this phase by the best (lowest energy) approximant model available to us, containing 128 atoms in a cubic unit cell with an edge length of about 12.6 Å, and a composition of $Al_{71.9}Pd_{21.9}Mn_{6.3}$.[44] The structure model is conventionally denoted as "1/1." All atoms are incorporated in the four PMI clusters and the four $Al_{12}Pd$ icosahedra, decorating the vertices of a canonical cell tiling.[45] The innermost shells of the PMI clusters in this icosahedral approximant are comprised of ten Al atoms, as opposed to our optimal ξ' phases, that contain only nine Al atoms in each inner PMI shell. In our final evaluation of the phase stability, this 1/1 approximant is unstable by only 7 meV/atom. As a competing model, we also computed total energies of two models reported in literature, but both had significantly higher energies.[46,47]

Currently there is no good estimate of total energies for the 12 Å decagonal phase. In our database the structure is represented by its approximant T-Al-Pd-Mn. In agreement with recent experimental work[48] composition and chemical ordering of the optimal low-temperature ternary structure is $Al_{31}Pd_2Mn_6$.[49] Both space group and the number of atoms in the unit cell are identical with the reported binary Al_3Mn high-temperature phase.[50]

The approximate compositions of the ε phases are shown in Fig. 4. Thus, our competing phases are T-Al-Pd-Mn, $Al_{21}Pd_8$,

TABLE II. Compositions, space groups, Pearson symbols, and energies of our optimized structures. The structures are listed in the same order as discussed in the paper. ΔE_{old} is the energy difference to our initial convex hull (cf. Fig. 4), ΔE_{new} is the energy difference relative to our new convex hull (cf. left part of Fig. 13). The relaxed atomic positions of structures 16, 17, 20, 21, and 25 are listed in Ref. 52.

	Structure	PMI shell	Space group (No.)	Pearson symbol	ΔE_{old} (meV/atom)	ΔE_{new} (meV/atom)	Total energy (eV/atom)
11	ξ-$Al_{55}Pd_{16}Mn_4$	Al_8	$P1$ (1)	$aP150$	42.5	45.8	−4.7523
12	ξ-$Al_{57}Pd_{16}Mn_4$	Al_9	$P\bar{1}$ (2)	$aP154$	13.9	17.6	−4.7537
13	ξ-$Al_{59}Pd_{16}Mn_4$	Al_{10}	$C12/c1$ (15)	$mC316$	12.6	16.0	−4.7293
14	ξ-$Al_{61}Pd_{16}Mn_4$	Al_{11}	$C1c1$ (9)	$mC324$	33.6	37.4	−4.6828
15	ξ-$Al_{56}Pd_{18}Mn_3$	Al_9	$Cmcm$ (63)	$oC308$	0.2	4.1	−4.7741
16	ξ-$Al_{56}Pd_{17}Mn_3$	Al_9	$Cmc2_1$ (36)	$oC304$	−3.9	0.4	−4.7476
17	ξ-$Al_{57}Pd_{16}Mn_3$	Al_9	$Cmc2_1$ (36)	$oC304$	−3.8	0.4	−4.7023
18	ξ-$Al_{54}Pd_{17}Mn_3$	Al_8	$P1$ (1)	$aP148$	28.0	31.9	−4.7426
19	ξ-$Al_{58}Pd_{17}Mn_3$	Al_{10}	$P1$ (1)	$aP156$	4.7	8.5	−4.7133
20	ξ'-$Al_{56}Pd_{17}Mn_3$	Al_9	$Pna2_1$ (33)	$oP304$	−4.3	0	−4.7480
21	ξ'-$Al_{57}Pd_{16}Mn_3$	Al_9	$Pna2_1$ (33)	$oP304$	−4.2	0	−4.7027
22	ξ-$Al_{57}Pd_{17}Mn_3$	Al_9	$Cmc2_1$ (36)	$oC308$	7.0	10.9	−4.7238
23	ξ-$Al_{58}Pd_{16}Mn_3$	Al_9	$Cmc2_1$ (36)	$oC308$	7.9	11.8	−4.6778
24	ξ'-$Al_{56}Pd_{19}$	Al_9	$Pna2_1$ (33)	$oP300$	16.6	16.6[a]	−4.5772
25	ξ_1'-$Al_{147}Pd_{44}Mn_8$	Al_9	$C1m1$ (8)	$mC796$	2.5	6.6	−4.7371
26	ξ_1'-$Al_{144}Pd_{47}Mn_8$	Al_9	$Amm2$ (38)	$oA796$	11.0	14.6	−4.7791
27	Ψ-$Al_{180}Pd_{53}Mn_{12}$	Al_{10}	$Amm2$ (38)	$oA1470$	35.0	38.5	−4.7429
28	$Al_{16}Pd_4Mn$	Al_{10}	$Pnma$ (62)	$oP168$	−8.5	−4.7	−4.6890

[a]The discovery of a new stable ternary structure does not affect the stability of a binary structure.

and either $Al_{12}Mn$ or Al_3Pd_2. Depending on the composition of the candidate structure, we will refer the energy difference ΔE to either tie triangle. Figure 13 includes the most important low-energy structures we optimized in this work. All optimized structures are further summarized in Table II.

In addition to the reported ternary phases, we also include a ternary version of the recently discovered quaternary structure $Al_{72}Pd_{18}Mn_5Si_5$,[51] with Si substituted by Al. According to our stability evaluations at $T = 0$ K, the structure is insignificantly more stable than our optimized ξ and ξ' phases (as shown in Fig. 13) and is discussed at the end of Sec. V.

B. Structural optimization of ξ and ξ' with respect to $T = 0$ K total energies

Our structure refinement is divided into two steps. In a first step we analyze the occupancies and occupancy correlations within the inner PMI shells. Determining the correct number of atoms contained within the inner shells is an important task, in which intuition easily fails. It is well known that quasicrystal-related Al-TM compounds often exhibit deep pseudogaps. The position of the Fermi level relative to the pseudogap center may have an important impact on the total energy (as we indeed show below), and is not dictated necessarily by local constraints. At the same time, the occupancy factors refined from diffraction data cannot be taken for granted, due to the couplings between Debye-Waller and occupancy factors. The loose inner shells with low symmetry encapsulated within the highly symmetrical outer shells of the PMI clusters may possess nearly continuous degrees of freedom connecting rather closely spaced alternative orientations of this inner cluster. A mix of such configurations is nearly impossible to represent by a few discrete sites available to a tractable refinement.

In a second step we vary the chemical ordering within the LBPP clusters. To make the optimization tractable, we assumed that the variations of the LBPP cluster especially on its fivefold axis are in the first-order approximation independent from the inner-PMI-shell cluster variations. As we show later, careful optimization of the chemical ordering along this cluster axis revealed striking impact on the total energy, and proved that the ξ and ξ' phases are stable down to zero temperature, according to our DFT approximated energetics. One of the counterintuitive findings was that the optimal chemical sequence along the LBPP fivefold axis places Mn-Pd atoms as nearest neighbors, a feature that we have never seen in other low-energy structures of the ternary Al-Pd-Mn compounds.

Finally, as already mentioned in Sec. II, there are some atomic sites reported in the diffraction refinement, located in the interstitial spaces between the PMI and LBPP clusters. Placement of these atoms is in apparent conflict with other Al atoms in the second PMI shells. We could never find a plausible low-energy configuration that would occupy these sites.

1. Occupancies of inner PMI shells

In this section we systematically minimize the total energy of the ξ phase with respect to (i) the number of Al atoms present in the inner PMI shells; (ii) optimal shape/orientations of these inner subclusters. The inner shells are encapsulated within nearly icosahedral second shells, and since they comprise less than 12 atoms, their symmetry is necessarily lower than the icosahedral one, leading to several possible orientations. The two constraints selecting among these inner-shell

orientations are vertical (along PMI stacking axis) and horizontal (perpendicular to PMI stacking axis) interactions between the PMI clusters. While the vertical interaction is pretty much separable and independent from column to column, the horizontal PMI-PMI interactions select the favorable spatial patterns of PMI columns.

The monoclinic unit cell of ξ contains four PMI clusters (two adjacent PMI columns, each with two clusters on top of each other). We start occupying each inner shell with 8 Al atoms, and gradually increase the number up to 11 Al atoms per PMI. In the following the TM(8) and TM(11) sites of the LBPP clusters are occupied by Mn and Al atoms, respectively, consistent with the Boudard model [cf. Fig. 1(b)]. The resulting structures contain 32 Pd and 8 Mn atoms, whereas the number of Al atoms varies from 110 for $4\times Al_8$, up to 122 for an inner-shell occupation of $4\times Al_{11}$. The relative stability of each model (ΔE from the appropriate tie triangle) is evaluated by constructing the convex hull from the enthalpies of formation ΔH of all binary subsystems as well as all ternary phases.

We found that the structures are most stable with either Al_9 or Al_{10} shells within each PMI cluster. The models are unstable by $\Delta E = 13.9$ and 12.6 meV/atom, respectively. Slightly higher energies were obtained for structures containing both Al_9 and Al_{10} shells, indicating an unfavorable interaction between both shells. The PMI clusters with Al_8 or Al_{11} inner shells are highly unfavorable. These structures were unstable by 42.5 and 33.6 meV/atom, respectively. The Al_8 inner shells were even unstable mechanically, since during the annealing process some atoms from the outer Al_{30} shells drifted inward, forming Al_9 shells. On the other hand, the inner shells seemed to be "overoccupied" with 11 Al atoms, as some atoms drifted toward the outer PMI shells in the course of the molecular dynamics annealing.

Shape of the inner shells. The PMI clusters obtained after relaxation are shown in Fig. 5. We observed two different types of Al_8 shells. One type of shell is a nearly perfect cube with edge lengths of 2.7–3.0 Å. The other type of shell can be described as a distorted square antiprism. The Al_9 shell is a trigonal prism, capped within a larger triangle (tricapped trigonal prism, TTP). Its threefold axis is aligned (approximately) along the pseudodecagonal (stacking) direction. The Al_{10} shells are best described by bicapped square antiprisms (BSA), where the twofold axes are oriented along the twofold axes of the outer PMI shells. The Al_9 and Al_{10} shells can point in different directions as outlined in Fig. 5. For instance, in Fig. 5 the threefold axis of the TTPs in the upper two PMI clusters point along the stacking axis, whereas the lower TTPs are aligned along a local fivefold axis. For the Al_{11} shells, no unique description can be established, as the shells had variable shape and complicated pattern of orientational relationship with respect to the second shell.

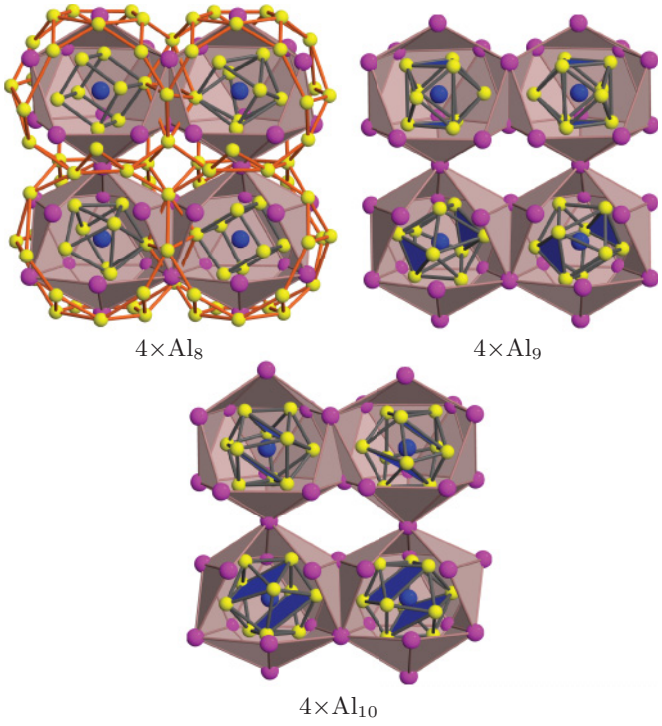

FIG. 5. (Color online) PMI clusters in ξ after relaxation. The vertical axis corresponds to the PMI stacking axis. The outer Al_{30} shells are shown only for the $4\times Al_8$ occupation. The triangles of the trigonal Al_9 shell and the antiprisms of the Al_{10} shells are shaded in blue to outline their threefold and twofold axes, respectively.

2. Chemical ordering within LBPP clusters

The inner-shell optimization reported in the previous section was performed using a fixed standard model for the chemical ordering within the LBPP cluster. In this second stage of the refinement, our strategy is to fix the energy-minimizing model for the inner shells, and refine the LBPP cluster interior. Due to the small energy difference between the structures containing Al_9 and Al_{10} shells, we accordingly split the LBPP optimization into two branches. Since the Al_9 variant proved more optimal, in the following, unless stated otherwise, the PMI clusters have Al_9 inner shells.

Our optimization first focuses on the atoms on the LBPP axis. As already mentioned, the LBPP cluster can alternatively be described in terms of separated spherical shells, similar to the PMI cluster. In both clusters the second shell consists of two subshells comprised of Al and Pd atoms. The inner part is either a pure Al_{8-11} shell (PMI), or a composite $Al_{10}Mn_2$ shell (LBPP). We believe it is more appropriate to change the chemical ordering within the LBPP cluster to obtain a similar atomic arrangement as in the PMI cluster. Therefore, we occupy the central TM(11) position of the LBPP cluster by Mn and replace the original Mn atoms located at the TM(8) sites by Pd as shown in Fig. 6(a). In doing so, we found a structure lying very close to the convex hull ($\Delta E = 0.2$ meV/atom). The first-neighbor Mn-Pd distances within the LBPP clusters are 2.86 Å and seem to be the key factor for the enhanced stability. The space group of this structure is *Cmcm* (No. 63). The unit cell contains 154 atoms in the primitive cell, with a composition $Al_{56}Pd_{18}Mn_3$. For comparison, the lowest-energy structure we found with the initial chemical ordering [see Fig. 1(b)] was unstable by $\Delta E = 12.6$ meV/atom.

We went one step further and broke the mirror symmetry of the LBPP cluster by replacing one of the Pd atoms within

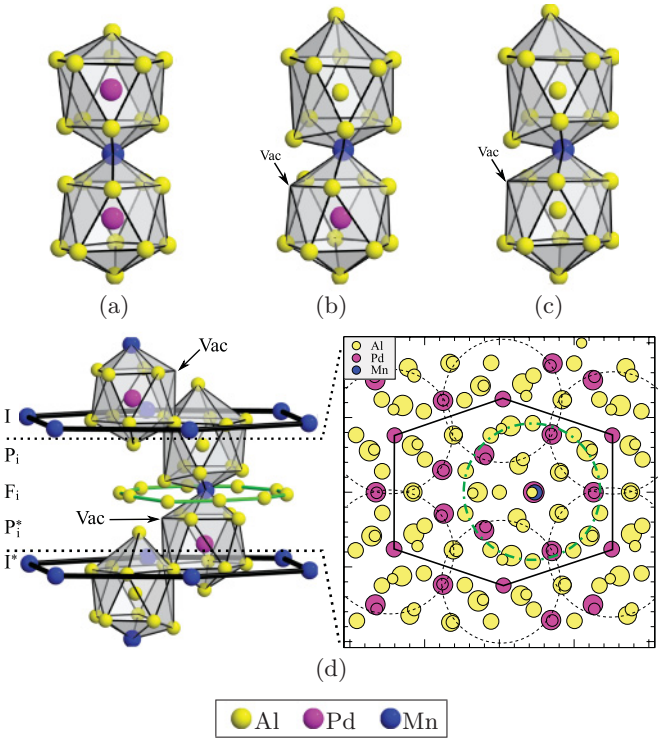

FIG. 6. (Color online) (a)–(c) Icosahedra of the LBPP clusters with different chemical orderings. The structure in (a) is unstable by 0.2 meV/atom. The structures in (b) and (c) are stable with respect to all competing phases. All three structures contain Al_9 inner shells in their PMI clusters. (d) Alignment of the LBPP cluster from (b) along the PMI stacking axis. Only atoms of the flat and adjacent puckered layers are displayed in the right picture. Larger circles indicate atoms sitting in lower layers. PMI clusters are outlined with dashed circles. The Al decagon located on the flat layer is outlined with a dash-dotted circle. The unoccupied sites in (b) and (c) correspond to Al(21) in Ref. 4. Vac means vacancy.

the icosahedra by Al. During the annealing certain Al atoms drifted toward the PMI clusters, resulting in some Al_{10} inner shells, and leaving one atomic site in each LBPP clusters unoccupied as shown in Fig. 6(b). The same behavior was observed when both TM(8) sites were occupied by Al [see Fig. 6(c)]. The structures were almost stable. We removed the diffused atoms in both structures to keep the inner PMI shells occupied with nine Al atoms, and repeated the annealings. Then both structures turned out to be stable with respect to all competing phases. Thus, our final optimal models of the ξ phase contain 152 atoms in the primitive cell, with two stable compositions $Al_{56}Pd_{17}Mn_3$ and $Al_{57}Pd_{16}Mn_3$, respectively. The space group of both structures is $Cmc2_1$ (No. 36).

The electronic density of states of the former structure is shown in Fig. 7. Its prominent feature is the broad and deep pseudogap. While models with Al_9 or Al_{10} shells have Fermi energies located near the center of the pseudogap, as required by the electronic stabilization mechanisms, models with unfavorable inner shells, as for instance Al_8, have Fermi energies shifted by about 0.3 eV relative to the pseudogap minimum.

Finally, we have applied these optimal decoration rules to the ξ' tiling, and relaxed the models until forces vanished. The

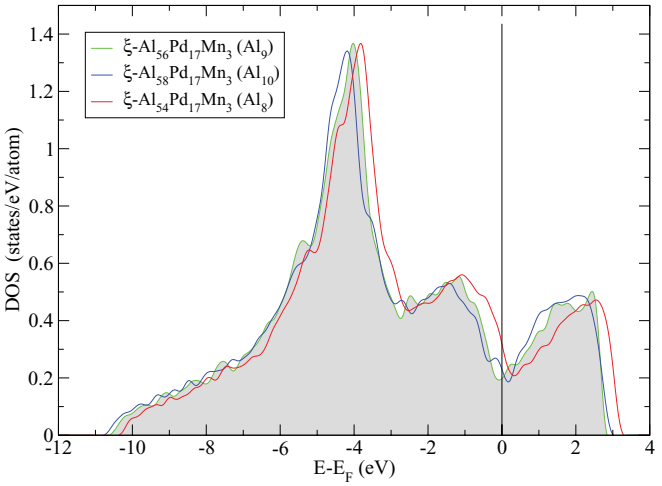

FIG. 7. (Color online) Comparison of the electronic density of states (DOS) of ξ with different inner PMI shells. The structure with Al_9 inner shells is stable with respect to the competing phases, whereas the structures with Al_8 and Al_{10} shells are unstable by 28.0 and 4.7 meV/atom, respectively.

resulting total energies were by 0.4 meV/atom lower than their ξ-tiling counterparts (for both stable compositions). The space group of both structures is $Pna2_1$ (No. 33). In Ref. 52 we list the relaxed atomic positions of our stable ξ and ξ' structures.

3. *Significance of the Al(9) atoms*

So far our models did not include the Al(9) atoms located outside the PMI and LBPP clusters (see Fig. 2). From the diffraction data refinement, the site was half-occupied by Al, but its occupancy conflicted with the pair of nearby (about 2.3 Å) Al(17) atoms, that were reported to be fully occupied. Nevertheless, for completeness we studied also various models in which this site gets occupied by an Al atom [while the conflicting Al(17) atoms were expected to adjust their position to avoid the short distance].

We observed that during the annealing these atoms drifted either into the PMI clusters and increased the occupancies of the inner shells, or into the LBPP clusters if there were any vacancies available. Only when the annealing temperature was kept as low as 300–500 K, the Al atoms remained at these Al(9) sites. In our stable models we fully occupied these sites and relaxed the coordinates until forces vanished. The structures were unstable by more than 7 meV/atom, corresponding to about 0.5 eV cost per Al(9) site. Possibly these sites are a feature of the high-temperature structure.

C. Internal degrees of freedom of inner PMI shells in ξ and ξ'

The Al_9 shells forming the core part of the PMI clusters have approximate trigonal $3/m$ symmetry, but they are encapsulated within an approximately icosahedral potential of the second PMI shells $Pd_{12}Al_{30}$. Due to this broken symmetry it is natural to expect that there must exist other, energetically nearly equivalent orientations of the Al_9 shell. On the other hand, there are two additional strong terms effectively lowering the symmetry of the potential inside the PMI: approximately pentagonal symmetry breaking due to having one fivefold axis

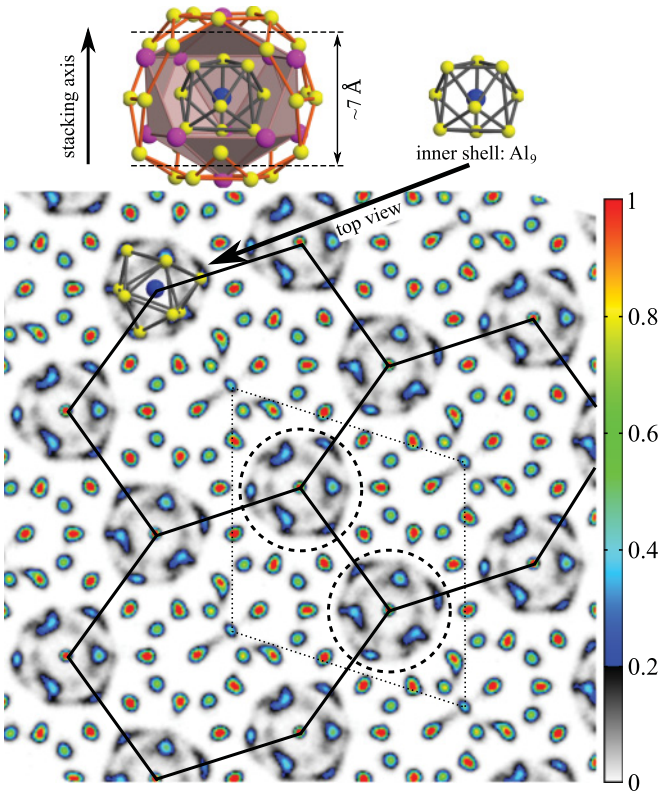

FIG. 8. (Color online) Density plot of the atoms in the ξ phase at 1200 K, time averaged after 50 ps. The density plot is projected along the PMI stacking axis. Dotted lines outline the unit cell, dashed circles outline the inner PMI shells. The upper part shows a single PMI cluster and its inner Al_9 shell: only atoms within the dashed lines are shown in the density plot. For the sake of clarity, one Al_9 shell is superimposed in the density plot.

parallel to the global pseudodecagonal (stacking) axis, and the PMI-PMI direct linkages, dictated by the arrangement of the PMI-cluster columns.

The vibrational and configurational degrees of freedom related to the reshufflings of the inner-shell atoms are activated at finite temperature, and certainly contribute to the free energy, providing a stabilization effect.

Here the dynamics of the inner shells has been studied in an *ab initio* molecular dynamics simulation at 1200 K in the NVT ensemble. A time-averaged density plot of a 7 Å thick slice containing one "layer" of PMI clusters, projected along to the PMI stacking axis, is shown in Fig. 8. The sharp red-yellow maxima correspond to the rigid part of the structure, with atomic positions concentrated around their unique equilibrium positions. The weaker, smeared blue-gray areas correspond to extremely mobile inner-shell atoms of the PMI clusters. While reshuffling, the atoms approximately maintain the trigonal prismatic shape of the shell, resulting in a kind of rotational motion: no distinct jumps could be observed.

To get a first estimate for the energy fluctuations as the inner-shell atoms reshuffle, we relaxed the high-temperature structure at different times to 0 K. The relaxed energies varied up to about 2 meV/atom. In all cases the threefold axes of the inner Al_9 shell pointed along a local fivefold axis of the outer PMI shells (not necessarily the stacking axis). In addition,

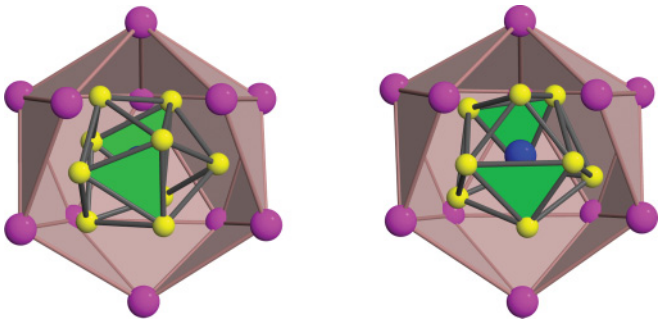

FIG. 9. (Color online) Snapshots of an inner PMI shell at different times after relaxation. The vertical fivefold axis is the stacking axis of the PMI clusters. The triangles of the trigonal prisms are highlighted in green to outline their threefold axis.

we found certain configurations where the same inner shell appeared slightly rotated with respect to the same fivefold axis as shown in Fig. 9.

Nevertheless, the time-averaged density plot indicates that the preferred orientations of the inner shells must be parallel to the stacking axis of the structure. In fact, in our lowest energy configurations the threefold axes of all inner shells point along the stacking direction.

V. DISCUSSION

A. ξ' in the binary Al-Pd system

In 1994 Matsuo *et al.*[34] reported on an approximant to a decagonal quasicrystal with 16 Å periodicity, designated Al_3Pd. The orthorhombic unit cell contained approximately 280 atoms occupying 300 sites, with lattice parameters $a = 23.36$ Å, $b = 12.32$ Å, and $c = 16.59$ Å, and space group $Pna2_1$. The structure is nearly identical to the ξ' phase. The main differences are the Mn sites that are substituted by Pd, and the inner PMI shells, which contain at most 8 Al atoms. A direct comparison of the atomic positions can be found in Ref. 4.

As in the ternary Al-Pd-Mn case, for the purpose of optimization of total energies we studied the binary ξ phase, rather than the ξ' phase. Interestingly, the interstitial Al(9) site of the Boudard model was also found in Al_3Pd [Al(21) in Ref. 34]. The occupancy factor was specified as 0.2. Similar to the ternary ξ and ξ' phase, we found that these atoms are evidently disfavored by our total energy calculations.

Varying the number of atoms in the inner PMI shells from eight to ten, we find that like in the ternary phase, the optimal shells are Al_9 with similar trigonal prismatic arrangements. The second modification that lowered the energy by 3 meV/atom was a removal of four Pd atoms from four PMI second shells.

The four PMI clusters contained in the primitive unit cell of this binary ξ phase are shown in Fig. 10(a). The Pd atoms were removed such that the vacancies are located next to each other in the hexagons [cf. Fig. 10(b)]. The centers of the LBPP clusters and the centers of the icosahedra within the LBPPs are all occupied by Pd: these three Pd atoms form a vertical chain with 2.86 Å distance to each other. The unit cell contains 112 Al and 38 Pd atoms, corresponding to a composition of about $Al_{74.7}Pd_{25.3}$. At 0 K the structure is by 15 meV/atom unstable to decomposition into fcc Al and $Al_{21}Pd_8$. At elevated

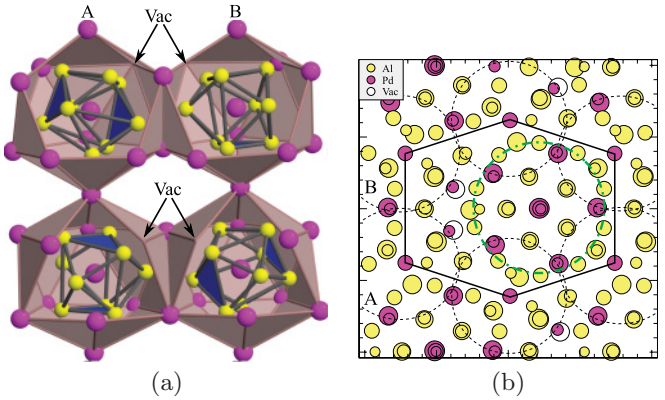

FIG. 10. (Color online) Optimized Al_3Pd structure. (a) Side view of PMI clusters with central Pd atoms, inner Al_9 and outer Pd_{11} shells. (b) Top view along the stacking axis of PMI clusters. Only atoms on the flat and its adjacent puckered layers are shown. PMIs are encircled with black-dotted lines. Color coding same as in previous figures.

temperatures, instead of fcc Al, the competing phase should be Al_4Pd. Interestingly, both of these phases are packings of Al_9Pd clusters that appear to be a distorted version of the Al_9Mn clusters found inside the PMI clusters of the ξ phase. The metastability of these binary ξ and ξ' phases is in agreement with the experimental data.

In the optimal structure described above, some Al_9Pd clusters are rotated such that their threefold axis is no longer parallel to the stacking direction of the structure, which is a result of molecular dynamics annealing. If we insisted they all aligned along the stacking axis, the structure is mechanically stable, and its symmetry would be consistent with the experimentally determined space group $Pna2_1$, but the energy would increase by another 2 meV/atom. Of course this agreement should be interpreted as accidental: even low-symmetry models may still belong to a finite-temperature ensemble with higher statistical symmetry.

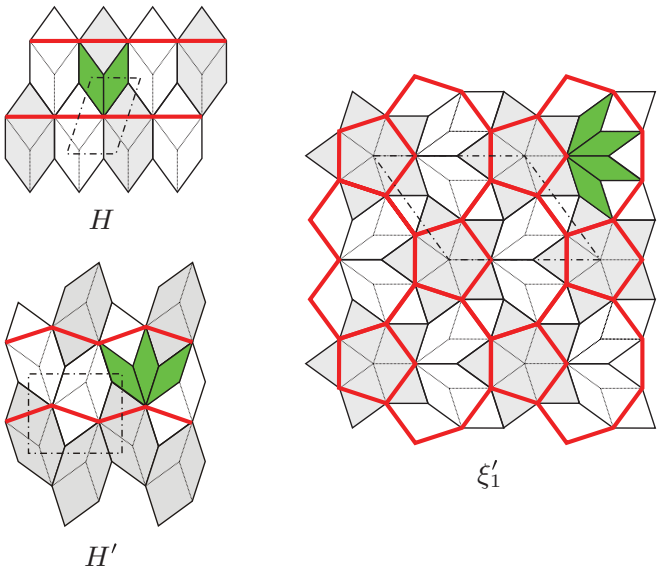

FIG. 11. (Color online) HBS-tiling models for the H, H', and ξ'_1 phases. The skinny rhombi are outlined to illustrate the different tile-tile interactions existing in each phase. See text for more details.

B. Toward phason-line models

The ε-phase family consists, apart from ξ and ξ', of a variety of other similar phases. These phases can be described by introducing an additional set of tiles, a banana-shaped nonagon, and a pentagon. As before, each vertex is a projection of the PMI clusters along their stacking axis. The tiles are always found attached to each other, and have been termed

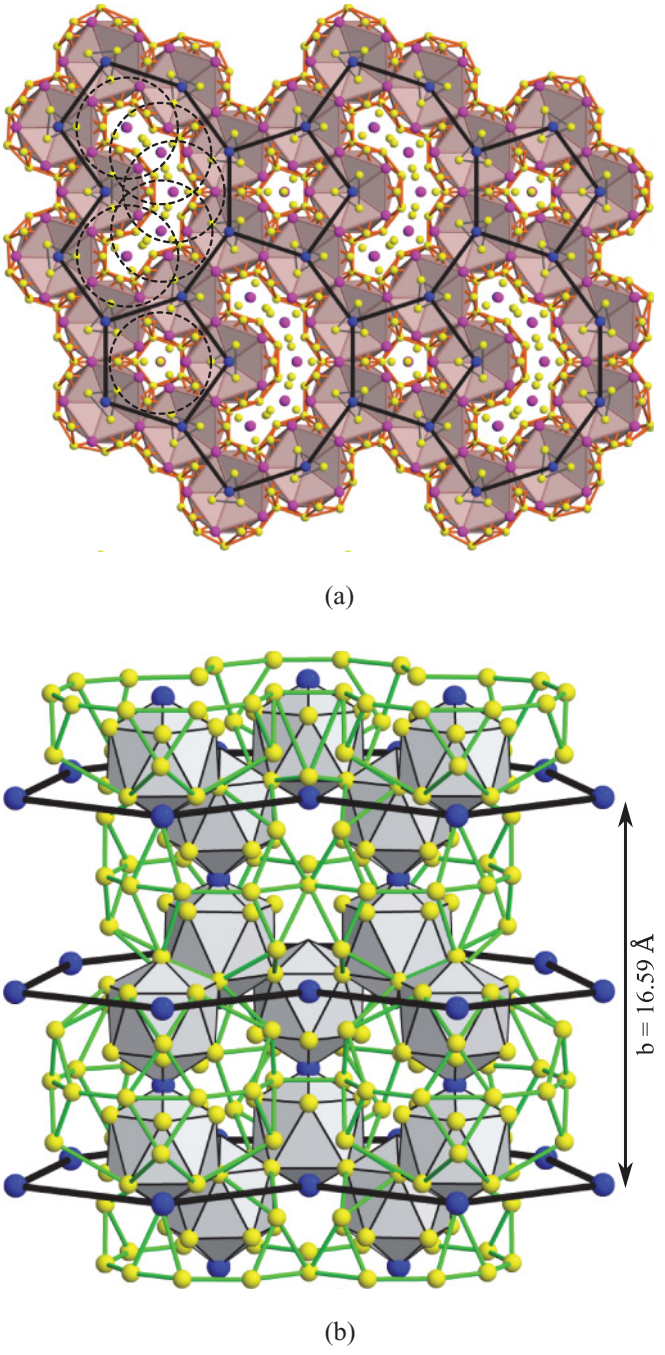

FIG. 12. (Color online) Optimized structure model for ξ'_1 with 398 atoms in the primitive unit cell. (a) Projection of the structure along the PMI stacking axis. Dashed circled outline the locations of the LBPP clusters. (b) Side view of one nonagon tile. The Pd_{10} pentagonal prisms and the PMI-cluster columns are omitted for the sake of simplicity. The nonagon contains five LBPP clusters per unit-cell height.

phason defect or phason line.[6] Periodic sequences of these phason lines are called phason planes.[53] The "larger" ε phases are distinguished by the number of hexagon rows that are sandwiched in between these phason planes. Their lattice parameters along the **a** and **b** directions are the same, whereas the **c** parameter depends on the number of inserted hexagon rows.[1] The simplest of these phases is ξ'_1 (ε_{16}) which contains exclusively phason planes with no hexagon tiles.

Only a few atomistic models exist in the literature describing these larger phases. No experimental structure refinements have been carried out yet, primarily due to the lack of good quality single crystals. Most investigations rely on the average structure of ξ'. Tian *et al.* constructed a Ψ phase by means of a *cut-and-shift* method of ξ'.[54,55] Thereby, two parts of the same ξ' structure are translated relative to each other. The model is confirmed by comparing the experimental and simulated high-resolution transmission electron microscopy images. More recently, a structure model for the ξ'_1 phase in the Al-Rh system has been proposed using a *strong-reflections approach*.[56] Similarly to Tian *et al.*, the atomic positions are deduced from those of the known ξ' phase. The space group of both models is $B2mm$ (No. 38).

Here we use the ξ'_1 phase to obtain a microscopic model for the phason lines. We construct the proper HBS tiling, and apply our optimized decoration motifs obtained from the low-temperature ξ and ξ' phases. In our HBS-tiling picture the pentagon is represented by a large star tile, and the nonagon by two hexagons (see Fig. 11). Within the tiling the skinny Penrose rhombi are located next to each other. This results in a direct contact of the LBPP clusters in the structure, a feature that is not present in ξ or ξ'.

Before tackling the chain of four skinny rhombi in ξ'_1, we constructed two other tilings in which the short diagonals of skinny rhombuses form infinite chains (see Fig. 11). Both tilings are composed of hexagon tiles only. Due to their similar arrangement with the hexagons in ξ and ξ', we termed these tilings H and H', respectively. The structure of H consists of PMI planes, formed by connecting adjacent PMI-cluster columns. The LBPP clusters, on the other hand, form further planes which are sandwiched in between the PMI planes. The primitive unit cell contains approximately 100 atoms. Similarly, the H' phase is simply an arrangement of staggered PMI planes, with the LBPP clusters located in between. The unit cell contains twice as many atoms as in the H phase. Both structures have not been observed in the experiment so far. Nevertheless, due to their rather small unit cells they offer a fast way to calculate total energies for a variety of decoration motifs. Afterwards, these motifs can be applied to the ξ'_1 phase, and hence to every other ε phase.

Our lowest-energy structure of the ξ'_1 phase contains nearly the same (symmetry-broken) LBPP clusters as our optimized ξ and ξ' models [cf. Fig. 6(b)]. The inner PMI shells are all occupied by nine Al atoms, forming the usual trigonal-prismatic shells. The banana-shaped nonagon comprises five entire LBPP clusters per unit cell height, as shown in Fig. 12. The nonagon tile, on the other hand, contains only one LBPP cluster per unit cell height. The structure is about 2.5 meV/atom above our convex hull. The primitive unit cell contains 294 Al, 88 Pd, and 16 Mn atoms. The space group is $C1m1$ (No. 8). The relaxed atomic positions of this structure can be found in Ref. 52.

Our highest-symmetry model for the ξ'_1 phase is unstable by 11 meV/atom. The space group is in agreement with the experimentally found ones. The structure is in principle the same as our best model, except for the LBPP clusters: here the Al atoms along the LBPP fivefold axis are substituted by Pd atoms [cf. Fig. 6(a)].

For comparison, we also relaxed the structure model for the Ψ phase, proposed by Tian *et al.*, with 540 Al, 159 Pd, and 36 Mn atoms in the primitive cell. According

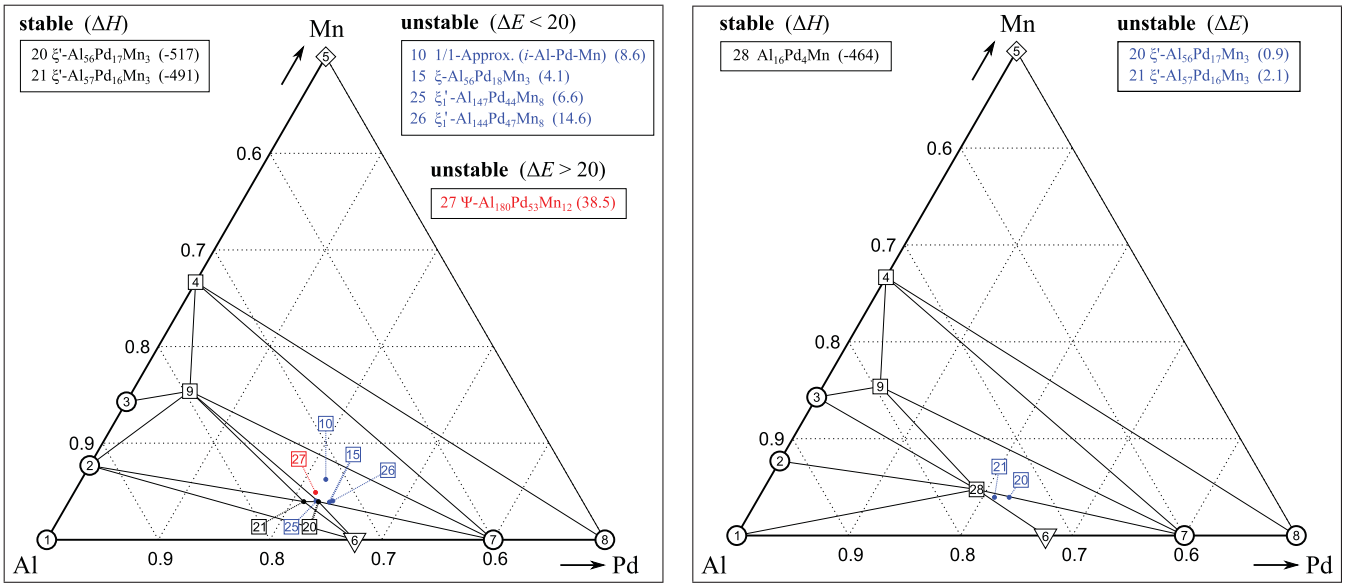

FIG. 13. (Color online) Low-temperature energy-phase diagrams of the Al-Pd-Mn system in the Al-rich corner with our optimized structures. The structures are labeled according to Tables I and II. Left: The two ξ' phases are stable down to $T = 0$ K with respect to all competing phases. The recently discovered $Al_{16}Pd_4Mn$ phase is not included in the stability evaluation. Right: If we include the $Al_{16}Pd_4Mn$ phase in our stability evaluations, both ξ' phases lie slightly above the convex hull.

to our DFT calculations, their model is unstable by more than 30 meV/atom with respect to our competing phases. This rather high energy difference is not surprising: in contrast to our models, their PMI clusters contain Al_{10} shells, as well as several (unfavored) interstitial atoms that are not covered by any cluster. The chemical orderings inside their LBPP clusters are also in contradiction to our optimized models. Furthermore, their banana-shaped nonagons contain only four LBPP clusters per unit cell height.

With the refined models for the flattened hexagons in ξ and ξ', and the optimized models for the phason lines, we are now able to construct all variants of the ε-phases family in the Al-P-Mn system. We believe that knowing the optimal decoration motifs for the fundamental tiles enables us to construct all other possible structures by simply changing the underlying tiling in our tiling-decoration model.

Table II summarizes all optimized structures discussed in this work by listing compositions, space groups, Pearson symbols, and energies. The structures are shown in the same order as appearing in Secs. IV B and V. Our new low-temperature energy-phase diagrams with the optimized structures are shown in Fig. 13. For completeness, we also include the recently discovered $Al_{72}Pd_{18}Mn_5Si_5$ phase in a separate phase diagram, with Si substituted by Al yielding a composition of $Al_{16}Pd_4Mn$. Surprisingly, the structure is stable down to $T = 0$ K, with respect to all competing phases including our optimized ξ' phases (see right part of Fig. 13). The calculated relative stability of this phase at $T = 0$ K does not change any of the conclusions about the optimal structure of the ε phases. It should also be remembered that our exploration of the low-temperature phase stability remains incomplete due to the absence of accurate models of the icosahedral Al-Pd-Mn phase.

VI. SUMMARY

We have systematically optimized the structures of the ξ and ξ' phases, and established all important correlations in chemical ordering and occupancies. The structure of these phases is best described as an assembly of two types of overlapping clusters, namely the pseudo-Mackay icosahedron and the so-called "large bicapped pentagonal prism." The fundamental clusters comprising almost 90% of all atoms are pseudo-Mackay icosahedra; they differ from the well known Mackay icosahedron cluster by a reduction of the occupancy and the symmetry of the inner shell, from 12 Al atoms (on the vertices of an icosahedron) to only 9 Al atoms forming trigonal-prismatic shells. For the secondary cluster we have determined the chemical ordering along its pentagonal axis which minimizes the energy of the structure. We found that the ξ and ξ' phases are, according to our calculations, stable down to $T = 0$ K (with a tiny preference for ξ'), and might even be a line compound, since we found two discrete stable compositions: $Al_{56}Pd_{17}Mn_3$ and $Al_{57}Pd_{16}Mn_3$. Both unit cells contain 152 atoms (corresponding to 304 in ξ'). In an *ab initio* molecular dynamics simulation we showed that the Al atoms of the Al_9 shells inside the PMI clusters are highly mobile which can lead to partial occupancy factors as obtained in the x-ray refinement.

A comparison has been made with the nearly isostructural Al_3Pd phase. The structure can be described by the same type of clusters. However, in contrast to the ternary phases, only metastable structures were found.

Using a tiling-decoration method we applied our optimized decoration motifs obtained from the refinement of the ξ and ξ' phases to a tiling representing the ε_{16} phase. This phase enabled us to investigate the structure of the phason defects in more detail. With these results we are now able to construct all variants of the ε-Al-Pd-Mn phases.

ACKNOWLEDGMENTS

This work has been supported by Deutsche Forschungsgemeinschaft, Paketantrag "Physical Properties of Complex Metallic Alloys" (PAK 36), TR-154/24-2. M.M. has been also supported by Slovak national Grants VEGA j2/0111/11 and APVV-0647-10.

*benjamin.frigan@itap.uni-stuttgart.de

[1] M. Heggen, M. Engel, S. Balanetskyy, H.-R. Trebin, and M. Feuerbacher, Philos. Mag. **88**, 507 (2008).
[2] V. Raghavan, J. Phase Equilib. Diffus. **30**, 71 (2009).
[3] H. Klein, M. Audier, M. Boudard, M. de Boissieu, L. Beraha, and M. Duneau, Philos. Mag. A **73**, 309 (1996).
[4] M. Boudard, H. Klein, M. D. Boissieu, M. Audier, and H. Vincent, Philos. Mag. A **74**, 939 (1996).
[5] L. Beraha, M. Duneau, H. Klein, and M. Audier, Philos. Mag. A **76**, 587 (1997).
[6] H. Klein, M. Feuerbacher, P. Schall, and K. Urban, Phys. Rev. Lett. **82**, 3468 (1999).
[7] The ξ'_n phases have large lattice constants, which—due to too high strain energies—prevent the existence of integer dislocations and admit only partial ones.
[8] M. Engel and H.-R. Trebin, Philos. Mag. **85**, 2227 (2005).
[9] M. Feuerbacher, H. Klein, and K. Urban, Philos. Mag. Lett. **81**, 639 (2001).
[10] M. Heggen and M. Feuerbacher, Mater. Sci. Eng. A **400-401**, 89 (2005), dislocations 2004.
[11] A. Katz and D. Gratias, J. Non-Cryst. Solids **153-154**, 187 (1993), proceedings of the Fourth International Conference on Quasicrystals.
[12] The number in parentheses specifies the space group according to the International Tables for Crystallography, Volume A: Space-Group Symmetry.
[13] M. Mihalkovič, W. J. Zhu, C. L. Henley, and M. Oxborrow, Phys. Rev. B **53**, 9002 (1996).
[14] F. Lançon and L. Billard, J. Phys. **49**, 249 (1988).
[15] J. Stadler, R. Mikulla, and H.-R. Trebin, Int. J. Mod. Phys. C **8**, 1131 (1997).
[16] M. S. Daw and M. I. Baskes, Phys. Rev. Lett. **50**, 1285 (1983).
[17] F. Ercolessi and J. B. Adams, Europhys. Lett. **26**, 583 (1994).
[18] P. Brommer and F. Gähler, Modell. Simul. Mater. Sci. Eng. **15**, 295 (2007).
[19] D. Schopf, e-print arXiv:1110.2038 (to be published).

[20]G. Kresse and J. Hafner, Phys. Rev. B **47**, 558 (1993).
[21]G. Kresse and J. Furthmüller, Phys. Rev. B **54**, 11169 (1996).
[22]G. Kresse and D. Joubert, Phys. Rev. B **59**, 1758 (1999).
[23]We use the standard PAW potentials, supplied with the VASP package: PAW_GGA Al 05Jan2001, PAW_GGA Pd 05Jan2001, PAW_GGA Mn 03Mar1998.
[24]J. P. Perdew and Y. Wang, Phys. Rev. B **45**, 13244 (1992).
[25]H. J. Monkhorst and J. D. Pack, Phys. Rev. B **13**, 5188 (1976).
[26]For the electronic minimization we use the blocked Davidson iteration scheme.
[27]C. B. Barber, D. P. Dobkin, and H. Huhdanpaa, ACM Trans. Math. Soft. **22**, 469 (1996).
[28]M. Mihalkovič and M. Widom, Phys. Rev. B **70**, 144107 (2004).
[29]M. Mihalkovič and M. Widom, Phys. Rev. B **75**, 014207 (2007).
[30]J. P. Perdew, K. Burke, and M. Ernzerhof, Phys. Rev. Lett. **77**, 3865 (1996).
[31]P. Villars, *Pearson's Handbook of Crystallographic Data for Intermetallic Phases* (ASM International, Materials Park, Ohio, 1997).
[32]H. Okamoto, J. Phase Equilib. **24**, 196 (2003).
[33]M. Wörle, F. Krumeich, T. Chatterji, S. Kek, and R. Nesper, J. Alloys Comp. **455**, 130 (2008).
[34]Y. Matsuo and K. Hiraga, Philos. Mag. Lett. **70**, 155 (1994).
[35]B. Grushko, M. Yurechko, and N. Tamura, J. Alloys Comp. **290**, 164 (1999).
[36]H. Klein, M. Durand-Charre, and M. Audier, J. Alloys Comp. **296**, 128 (2000).
[37]M. Mihalkovič and M. Widom, Alloy Database: [http://alloy.phys.cmu.edu].
[38]A. Tsai, A. Inoue, and T. Masumoto, Philos. Mag. Lett. **62**, 95 (1990).
[39]M. Boudard, M. de Boissieu, C. Janot, G. Heger, C. Beeli, H.-U. Nissen, H. Vincent, R. Ibberson, M. Audier, and J. M. Dubois, J. Phys. Condens. Matter **4**, 10149 (1992).
[40]C. Beeli, H. Nissen, and J. Robadey, Philos. Mag. Lett. **63**, 87 (1991).
[41]H. Klein, M. Boudard, M. Audier, M. D. Boissieu, H. Vincent, L. Beraha, and M. Duneau, Philos. Mag. Lett. **75**, 197 (1997).
[42]L. Beraha, M. Duneau, H. Klein, and M. Audier, Philos. Mag. A **78**, 345 (1998).
[43]L. Barbier, D. Le Floc'h, Y. Calvayrac, and D. Gratias, Phys. Rev. Lett. **88**, 085506 (2002).
[44]M. Mihalkovič, M. Krajči, C. L. Henley, and J. Hafner (unpublished).
[45]C. L. Henley, Phys. Rev. B **43**, 993 (1991).
[46]A. Quandt and V. Elser, Phys. Rev. B **61**, 9336 (2000). V. Elser, Philos. Mag. B **73**, 641 (1996).
[47]E. S. Zijlstra, S. K. Bose, M. Klanjšek, P. Jeglič, and J. Dolinšek, Phys. Rev. B **72**, 174206 (2005); E. S. Zijlstra, S. K. Bose, and J. Dolinšek, *ibid*. **72**, 092203 (2005).
[48]S. Balanetskyy, G. Meisterernst, M. Heggen, and M. Feuerbacher, Intermetallics **16**, 71 (2008).
[49]M. Krajči and M. Mihalkovič (unpublished).
[50]K. Hiraga, M. Kaneko, Y. Matsuo, and S. Hashimoto, Philos. Mag. B **67**, 193 (1993).
[51]R. Simura, N. Kaji, K. Sugiyama, and K. Hiraga, Philos. Mag. **91**, 2603 (2011).
[52]See Supplemental Material at http://link.aps.org/supplemental/10.1103/PhysRevB.84.184203 for the relaxed atomic positions in CIF format.
[53]H. Klein and M. Feuerbacher, Philos. Mag. **83**, 4103 (2003).
[54]H. Tian, W. Sun, and Z. Zhang, Philos. Mag. Lett. **86**, 309 (2006).
[55]H. Tian, W. Sun, and Z. Zhang, Philos. Mag. Lett. **86**, 539 (2006).
[56]M. Li, J. Sun, P. Oleynikov, S. Hovmöller, X. Zou, and B. Grushko, Acta Crystallogr. Sect. B **66**, 17 (2010).